SIX DAYS ■ THREE CONFERENCES ■ ONE EXHIBITION

EUROPEAN MICROWAVE WEEK 2019
PARIS EXPO PORTE DE VERSAILLES, PARIS, FRANCE
1 place de la Porte de Versailles
29TH SEPTEMBER - 4TH OCTOBER 2019

EuMW 2019
UN|VERSAL|TY THROUGH M|CROWAVES

EUROPEAN MICROWAVE WEEK
PORTE DE VERSAILLES
PARIS, FRANCE
29TH SEPT - 4TH OCT 2019
www.eumweek.com

EUROPEAN MICROWAVE WEEK 2019

CONFERENCE PROGRAMME

EUROPE'S PREMIER MICROWAVE, RF, WIRELESS AND RADAR EVENT

Register online at:

www.eumweek.com

EuMA
European Microwave Association

Official Publication: Microwave Journal

Organised by: horizon house

Supported by: IET The Institution of Engineering and Technology

Co-sponsored by: MTT-S

Co-sponsored by: IEEE

EuMIC 2019
The 14th European Microwave Integrated Circuits Conference
Co-sponsored by:
Electron Devices Society

49th European Microwave Conference 2019
The 49th European Microwave Conference
Co-sponsored by:
EurAAP

EuRAD 2019
The 16th European Radar Conference
Co-sponsored by:
EurAAP AESS

E04

EuMC12
MEMS, Phase-Change and Oxide Material Devices

Chair: Andrei Muller[1]
Co-Chair: Rolf Jakoby[2]
[1]École polytechnique fédérale de Lausanne (EPFL), [2]TU Darmstadt, IMP

08:30 - 08:50 *EuMC12-1*
MEMS Switches for mm-Wave Applications
Romain Stefanini[1]
[1]AirMems

08:50 - 09:10 *EuMC12-2*
A Compact Radial Divider Combiner for High power MEMS Switches
Rami Daher[1], Pierre Blondy[1]
[1]XLIM Research Institute, University of Limoges, Limoges, France

09:10 - 09:30 *EuMC12-3*
A Millimiter Wave High-Power RF MEMS Switch Based on Two Membranes in Parallel
Clement Dorion[1,2], Pierre Blondy[1], Valerie Madrangeas[1], Abedel-Halim Zahr[2], Ling-Yan Zhang[2], Areski Ghalem[2], Aurélien Beneteau[2], Maxime Rabanne[2], Romain Stefanini[2]
[1]XLIM Research Institute - UMR CNRS 7252, [2]AirMems

09:30 - 09:50 *EuMC12-4*
A Miniaturized Monolithic PCM Based Scalable Four-Port RF Switch Unit-Cell
Tejinder Singh[1], Raafat Mansour[1]
[1]University of Waterloo

09:50 - 10:10 *EuMC12-5*
All-Oxide Thin Film Varactor: From Test Structure to SMD Component
Dominik Walk[1], Daniel Kienemund[1], Patrick Salg[2], Lukas Zeinar[2], Aldin Radetinac[2], Philipp Komissinskiy[2], Lambert Alff[2], Rolf Jakoby[1], Holger Maune[1]
[1]TU Darmstadt, IMP, [2]TU Darmstadt, ATFT

E05

EuMC13
Planar Filters I

Chair: Cristiano Tomassoni[1]
Co-Chair: Jerzy Michalski[2]
[1]University of Perugia, [2]SpaceForest Ltd.

08:30 - 08:50 *EuMC13-1*
Microwave Filter Manufactured on Conventional or Innovative Technologies
Alexandre Manchec[1]
[1]Elliptika

08:50 - 09:10 *EuMC13-2*
Back-to-Back Connected Multiplexers for a Broadband Channel Splitter and Channel Combiner
Sanghoon Shin[1], Eric J. Naglich[2], Luciano Boglione[1]
[1]U.S. Naval Research Laboratory, [2]Booz Allen Hamilton

09:10 - 09:30 *EuMC13-3*
Ultra-Wideband Bandpass Filter Using Solder-Mask-Based Multilayer Technology
Hassan Bouazzaoui[1], Alexandre Manchec[1], Rozenn Allanic[2], Cédric Quendo[2], Benjamin Potelon[2], Florent Karpus[3]
[1]Elliptika [GTID], [2]Lab-STICC-Université de Bretagne Occidentale, [3]Protecno [GTID]

09:30 - 09:50 *EuMC13-4*
Direct Synthesis of Quad-Band Band-Pass Filter by Frequency Transformation Methods
Yi Wu[1], Erwan Fourn[1], Philippe Besnier[1], Cédric Quendo[2]
[1]Institut d'électronique et de télécommunications de Rennes, IETR, [2]Lab-STICC

09:50 - 10:10 *EuMC13-5*
Design of a Substrate Integrated Half Mode Coaxial Cavity Filter with Multiple Transmission Zeros
Satya Krishna Idury[1], Soumava Mukherjee[1]
[1]Indian Institute of Technology Jodhpur

E06

EuMC14
Focused Session Electromagnetic Methods for Monitoring and Manipulating Cells and Tissues

Chair: Francesca Apollonio[1]
Co-Chair: Maxim Zhadobov[2]
[1]ICEmB at DIET University of Rome Sapienza, [2]CNRS, Institut d'Électronique et de Télécommunications de Rennes, UMR–6164

08:30 - 08:50 *EuMC14-1*
Millifluidic Sensor Dedicated to the Microwave Dielectric Spectroscopy of Liquids
Patricio Felipe Jaque Gonzalez[1], Katia Grenier[1], David Dubuc[1], Thierry Veronese[2]
[1]LAAS-CNRS, [2]Ovalie-Innovation

08:50 - 09:10 *EuMC14-2*
Ultra-wideband Electrical Sensing of Nucleus Size in a Live Cell
Xiaotian Du[1]
[1]Lehigh University

09:10 - 09:30 *EuMC14-3*
A Microdosimetric Realistic Model to Study Frequency-Dependent Electroporation in a Cell with Endoplasmic Reticulum
Annalisa De Angelis[1], Agnese Denzi[1], Caterina Merla[2], Tomas Garcia-Sanchez[3], Franck André[3], Lluis Mir[3], Francesca Apollonio[1], Micaela Liberti[1]
[1]ICEmB@DIIET, University of Rome Sapienza, [2]ENEA, SSPT - Division of Health Protection Technologies, Rome, Italy, [3]CNRS, Univ. Paris-Sud, Université Paris-Saclay, Gustave Roussy, Villejuif, France

09:30 - 09:50 *EuMC14-4*
Radiation Performance of Highly Miniaturized Implantable Devices
Denys Nikolayev[1], Maxim Zhadobov[2], Wout Joseph[3], Luc Martens[3], Ronan Sauleau[2]
[1]École polytechnique fédérale de Lausanne (EPFL), Microwaves and Antenna Group, [2]CNRS, Institut d'Électronique et de Télécommunications de Rennes, UMR–6164, [3]imec / Ghent University

09:50 - 10:10 *EuMC14-5*
Numerical Investigations of CW Electric Fields on Lipid Vesicles for Controlled Drug Delivery
Laura Caramazza[1], Annalisa De Angelis[1], Elena Della Valle[2], Agnese Denzi[1], Martina Nardoni[3], Patrizia Paolicelli[3], Stefania Petralito[3], Francesca Apollonio[1], Micaela Liberti[1]
[1]ICEmB at DIET University of Rome Sapienza, [2]BioElectronic Vision Lab University of Michigan, [3]Department of Drug Chemistry and Technology, "Sapienza" University of Rome

E07

EuMC15
Antennas for Communication

Chair: Ioan Lager[1]
Co-Chair: Tobias Chaloun[2]
[1]Delft University of Technology, [2]University Ulm

08:30 - 08:50 *EuMC15-1*
Compact, Two-Port, Slot, Antenna for Dual-Band WiFi 2x2 MIMO Applications
Abdullah Haskou[1], Anthony Pesin[1], Jean-Yves Le Naour[1], Ali Louzir[1]
[1]Technicolor Research and Innovation

08:50 - 09:10 *EuMC15-2*
Compact, Integrated, Four-Sector, Antenna for Sub-6GHz 5G Indoor Access and Content Distribution over WiFi
Abdullah Haskou[1], Anthony Pesin[1], Jean-Yves Le Naour[1], Ali Louzir[1]
[1]Technicolor Research and Innovation

09:10 - 09:30 *EuMC15-3*
Characterization of a Low-Profile Quad-Feed Based Transmitarray Antenna at V-Band
Antonio Clemente[1], Maciej Smierzchalski[1], Mathieu Huchard[2], Cyril Barbier[2], Thierry Le Nadan[2]
[1]CEA LETI, [2]Radiall

09:30 - 09:50 *EuMC15-4*
High Self-Interference Cancellation Antenna for In-Band Full Duplex Communication System
Girdhari Chaudhary[1], Junhyung Jeong[1], Phanam Pech[1], Phirun Kim[1], Yongchae Jeong[1]
[1]Chonbuk National University

09:50 - 10:10 *EuMC15-5*
Compact Wideband CPW-fed Tri-Band Antenna With Multi-shaped Strips for WLAN/WiMAX Applications
Binyun Yan[1], Weixing Sheng[1], Jie Cui[1], Jie Lu[1]
[1]Nanjing University of Science and Technology

High Self-Interference Cancellation Antenna for In-Band Full Duplex Communication System

Girdhari Chaudhary[#1], Junhyung Jeong[#], Phanam Pech[#], Phirun Kim[#], and Yongchae Jeong[#2]

[#]Division of Electronics and Information Engineering, Chonbuk National University, Republic of Korea

[1]girdharic@jbnu.ac.kr, [2]ycjeong@jbnu.ac.kr

***Abstract* — This paper demonstrates a dual-polarized microstrip patch antenna with high interport isolation for in-band full duplex transceiver. The proposed antenna consists of four port linearly polarized signal radiating elements with differential feedings at input/output ports. The defected ground structure (DGS) under patch has been adopted for enhancement of antenna return loss bandwidth. To achieve high isolation, two identical differential feeding networks using wideband branch-line Balun have been utilized as a self-interference circuit. The analytical design equations have been derived for achieving high isolation in the proposed antenna. For experimental verification, the prototype has been fabricated at the center frequency of 2.5 GHz. The fabricated antenna provides more than 47 dB RF isolation between TX-to-RX port for 100 MHz bandwidth.**

***Keywords* — Branch-line Balun, differential feeding networks, high RF isolation, in-band full duplex.**

I. Introduction

In recent years, mobile data-traffic has been increasing rapidly. To achieve demand for high mobile data-traffic, system capacity enhancement has been regarded the most important requirement of a next-generation 5G communication network, which can be achieved by boosting spectral efficiency. Since in-band full duplex (IBFD) can simultaneously transmit and receive signals over the same time and frequency, IBFD can theoretically double data throughputs and spectral efficiency. Therefore, the IBFD system is considered as one of the candidates for next-generation 5G communication systems [1]. The major challenge for implementing IBFD systems is how to reduce the strong self-interference (SI) imposed on the received (RX) signals by the transmitted (TX) signals. The amount of self-interference cancellation (SIC) depends on the TX signal power, signal bandwidth, and the noise at the receiver [1]-[4].

In order to realize the advantages of the IBFD system, the SI signal level should be reduced to the same level as the receiver noise. In recent years, a lot of research has gone toward different SIC techniques to achieve desired cancellation [5]-[8]. Based on literature reviews, SIC can be achieved in three ways: cancellation at antenna stage or passive suppression, RF analog cancellation, and digital cancellation. In addition, the SIC should achieve higher than 50 dB with passive suppression (antenna stage) or RF analog stage in order to prevent the saturation of the receiver building blocks (low noise amplifier, mixer, and ADC).

The SIC technique at the antenna stage is the first step to achieving high levels of SIC, which can prevent saturation of the receiver. In addition, high RF isolation at the antenna stage make other stage cancellations easier without the need for complex RF analog and digital domain SIC techniques. One approach at antenna stage is to make use of orthogonal polarization to obtain high isolation between TX-and RX-ports [9]. In [10], a dual-polarized patch antenna is presented using a differential feeding network that consists of a power divider with two meandering strips with a 180^{o} phase difference to achieve 40 dB isolation between TX- and RX-ports. Similarly, a dual-polarized patch antenna with the hybrid ring feeding is present in [11], which provides measured isolation of more than 40 dB. In [12], a patch antenna is fed from the same edge where the dual-polarization is obtained by differential excitation of the two side ports with 180^{o} ring hybrid. However, the achievable isolation is limited because of the strong coupling between the closely-spaced microstrip feeding the radiating patch from the same edge. Furthermore, the dual-polarized with differential feeding patch antennas are presented in [13], [14] based on three and four ports, respectively. Although high isolation is obtained in these works, however, the bandwidth is still limited to 50 MHz at 2.4 GHz center frequency.

In this paper, the dual-polarized antenna with defected ground structure (DGS) has been demonstrated for IBFD transceiver using two identical wideband branch-line Balun feeding networks for achieving high TX-to-RX port isolation over wide frequency bandwidth. The general design equations have been derived to assist in the accurate design of the high isolation antenna.

II. Analytical Design Equations

Fig. 1 depicts the proposed structure of the double differential feeding antenna with wideband high isolation between TX- and RX-ports. The proposed antenna consists of a square shape single radiating patch where TX- and RX-operational modes are excited by the differential mechanism through a pair of opositively placed ports using Baluns. The DGS has been utilized at the bottom plane of the antenna for enhancing the reflection coefficients of the antenna. Signal flow analysis is applied to derive TX-to-RX isolation. First, input TX-signal is divided into two out-of-phase signals defined as (1) due to Balun B1.

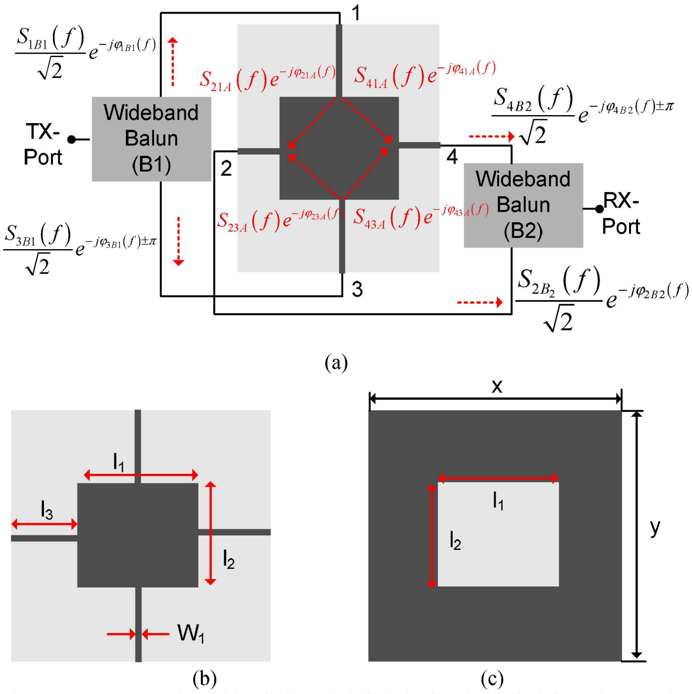

Fig. 1. (a) Proposed double differential fed dual-polarized defected ground (DGS) antenna for in-band full duplex system, (b) top view, and (c) bottom view of the antenna.

$$S_{Tx-1}(f)=\frac{S_{1B_1}(f)e^{-j\varphi_{1B1}(f)}}{\sqrt{2}},S_{Tx-2}(f)=\frac{S_{3B_1}(f)e^{-j\varphi_{3B1}(f)\pm\pi}}{\sqrt{2}} \quad (1)$$

Secondly, leakage signals generated from TX-antenna will be coupled with differential feeding network and combined by Balun B2 at RX-port of the antenna. Therefore, a coupling between TX-to-RX ports can be calculated as (2).

$$\Delta^{TX-RX}_{coupling}=\left[\begin{array}{l}\left\{\begin{array}{l}S_{Tx-1}(f)S_{21A}e^{-j\varphi_{21A}(f)}\\+S_{Tx-2}(f)S_{23A}(f)e^{-j\varphi_{23A}(f)}\end{array}\right\}\frac{S_{2B_2}(f)}{\sqrt{2}}e^{-j\varphi_{2B2}(f)}\\\left\{\begin{array}{l}S_{Tx-1}(f)S_{41A}e^{-j\varphi_{41A}(f)}\\+S_{Tx-2}(f)S_{43A}(f)e^{-j\varphi_{43A}(f)}\end{array}\right\}\frac{S_{4B_2}(f)}{\sqrt{2}}e^{-j\varphi_{4B2}(f)\pm\pi}\end{array}\right] \quad (2)$$

where $S_{ijA}(f)$ and $\varphi_{ijA}(f)$ are magnitude and phase of leakage signals generated through TX-mode operation of the antenna, respectively. Assuming lossless feeding networks (B1 and B2) are lossless and identical, the TX-to-RX ports isolation can be further simplified as (3) by using (1) and (2).

$$\Delta^{TX-RX}_{ISO}(f)=2\Big/\sqrt{b_1^2+b_2^2} \quad (3)$$

where

$$b_1=\left[\begin{array}{l}1-\Delta_{2A}\Delta_{B1}\cos(\Delta\varphi_{B1}+\Delta\varphi_{2A})-\Delta_{B2}\cos\Delta\varphi_{B2}\\+\Delta_{B1}\Delta_{B2}\Delta_{4A}\cos(\Delta\varphi_{B2}+\Delta\varphi_{B1}+\Delta\varphi_{4A})\end{array}\right] \quad (4a)$$

$$b_2=\left[\begin{array}{l}\Delta_{2A}\Delta_{B1}\sin(\Delta\varphi_{B1}+\Delta\varphi_{2A})+\Delta_{B2}\sin\Delta\varphi_{B2}\\-\Delta_{B1}\Delta_{B2}\Delta_{4A}\sin(\Delta\varphi_{B1}+\Delta\varphi_{B_2}+\Delta\varphi_{4A})\end{array}\right] \quad (4b)$$

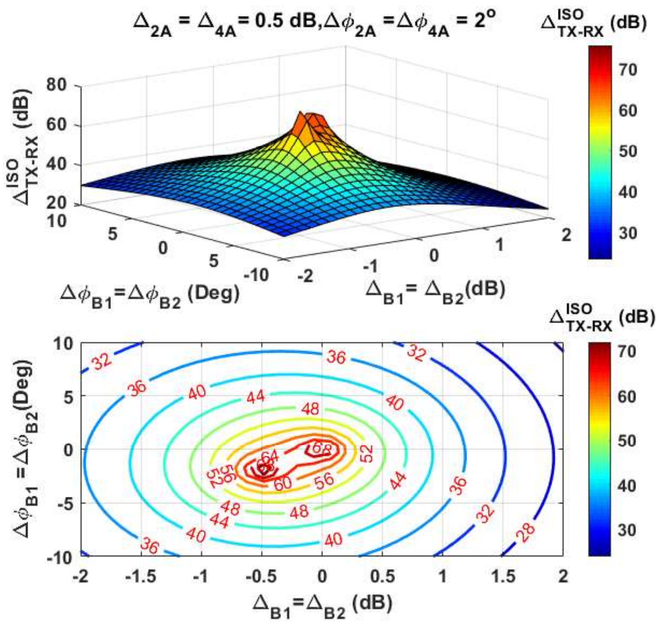

Fig. 2. Calculated Tx-to-Rx isolation of the proposed antenna.

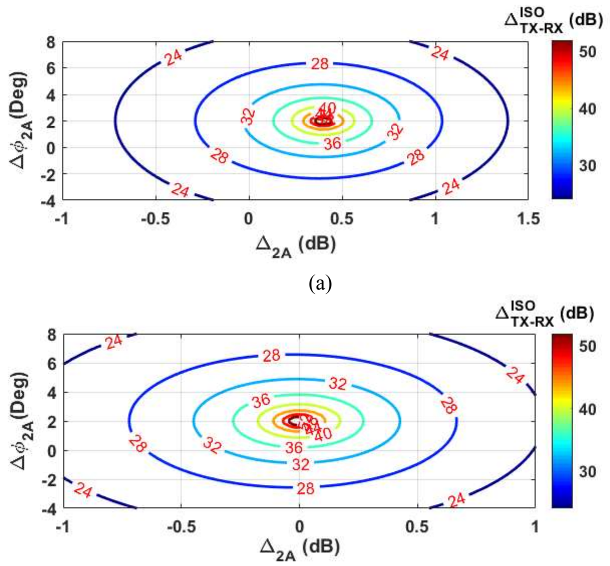

(b)

Fig. 3. Calculated TX-to-RX isolation for perfect feeding networks and different leakage antenna signal magnitude and phase variations: (a) Δ_{4A} = 0.4 dB, $\Delta\varphi_{4A}$ = 2° and (b) Δ_{4A} = 0 dB, $\Delta\varphi_{4A}$ = 2°.

$$\Delta_{B1}=|S_{3B_1}(f)|/|S_{1B_1}(f)|,\Delta_{B2}=|S_{4B2}(f)|/|S_{2B2}(f)| \quad (4c)$$

$$\Delta_{2A}=|S_{23A}(f)|/|S_{21A}(f)|,\Delta_{4A}=|S_{43A}(f)|/|S_{41A}(f)| \quad (4d)$$

$$\Delta\varphi_{B1}=\varphi_{3B1}(f)-\varphi_{1B1}(f),\Delta\varphi_{2B2}=\varphi_{4B2}(f)-\varphi_{2B2}(f) \quad (4e)$$

$$\Delta\varphi_{4A}=\varphi_{43A}(f)-\varphi_{41A}(f),\ \Delta\varphi_{4A}=\varphi_{43A}(f)-\varphi_{41A}(f) \quad (4f)$$

From (3), it can be concluded that TX-to-RX ports isolation of antenna depends only antenna leakage signals imbalances but also depends on feeding networks imbalances. Furthermore, the TX-to-RX isolation can be simplified as (5) if both feeding

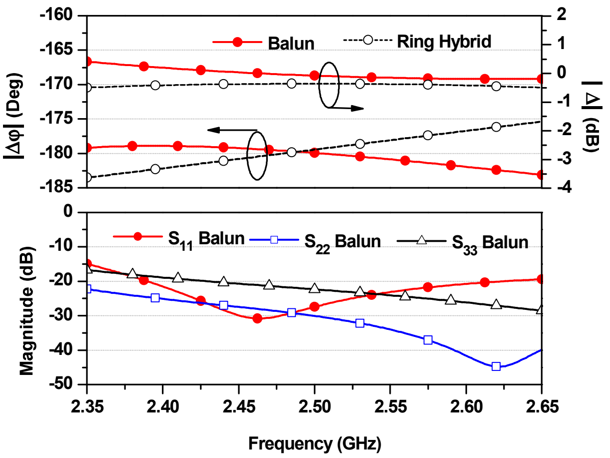

Fig. 4. Responses of differential feeding networks (DFNs).

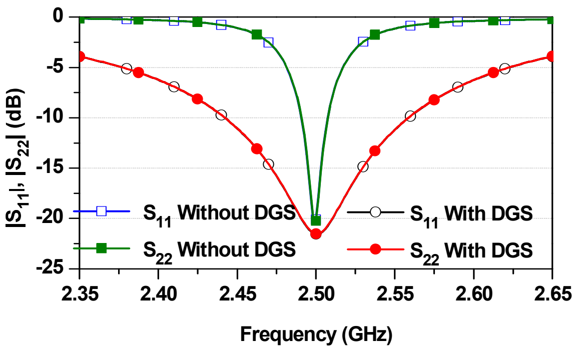

Fig. 5. Simulated $|S_{11}|$ and $|S_{22}|$ of the antenna with and without defected ground structure (DGS).

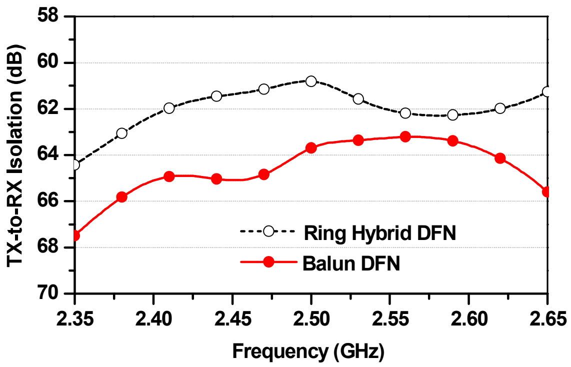

Fig. 6. Simulated TX-to-RX isolation of the proposed antenna with different differential feeding networks.

networks have perfect magnitude and phase imbalances.

$$\Delta_{ISO}^{TX-RX}(f) = 2 \Big/ \sqrt{\Delta_{2A}^2 + \Delta_{4A}^2 - 2\Delta_{4A}\Delta_{2A}\cos(\Delta\varphi_{2A} - \varphi_{4A})} \quad (5)$$

As can be seen from (5), the antenna leakage signal magnitude and phase should be equal to get infinite TX-to-Rx isolation of antenna. Therefore, these leakage signal magnitude and phase errors should be minimized for achieving the high isolation over the wide bandwidth.

For validation of the analytical equations, Figs. 2 and 3 show the calculated TX-to-RX isolation of IBFD antenna under different parameters variations. As observed from these figures, the high isolation over wide frequency bandwidth can be achieved if antenna leakage signals amplitude and phase errors of both feeding networks are minimum. In addition, the TX-to-RX isolation higher than 60 dB can be achieved if the amplitude and out-of-phase imbalance errors of feeding networks and antenna leakage signals are maintained within 0.2 dB and 2°, respectively.

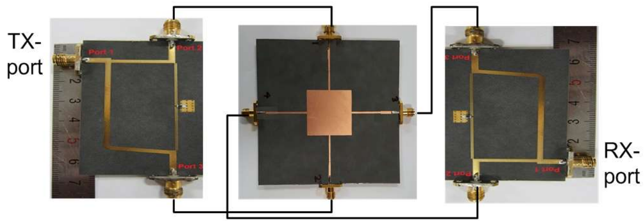

Fig. 7. Measurement setup of the proposed antenna.

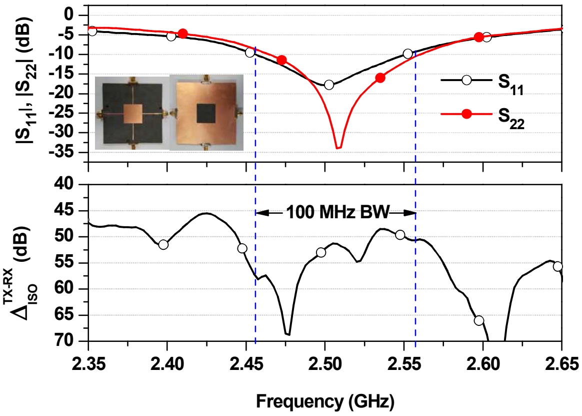

Fig. 8. Measured $|S_{11}|$, $|S_{22}|$, and TX-to-RX isolation of fabricated overall antenna.

Fig. 4 shows the characteristics of different feeding networks for comparison. As seen from this figure, the wideband branch-line Balun feeding network has superior performances as compared to the conventional ring hybrid [15]. Therefore, in this work, wideband branch-line will be utilized to achieve high isolation over the wide frequency bandwidth.

III. Simulation And Experimental Results

For experimental demonstration, the antenna is fabricated at the center frequency of 2.5 GHz using a substrate ($\varepsilon_r = 2.2$, $h = 0.787$ mm, and $\tan\delta = 0.0009$). The simulation is performed using ANSYS 2018. The patch size of the antenna is 30 × 30 mm^2.

Fig. 5 shows the simulated magnitudes of $|S_{11}|$ and $|S_{22}|$ with and without DGS, where the return loss of the proposed antenna with DGS is wider than without DGS. Similarly, Fig. 6 shows the simulated TX-to-RX isolation using different differential feeding networks. From these results, TX-to-RX isolation is higher over the wide frequency bandwidth in case of the wideband branch-line Balun feeding network because the magnitude and phase responses of Balun are superior to the ring hybrid.

The measurements were performed in a laboratory environment and the results were taken directly from a full-assembled antenna system as shown in Fig. 7. Fig. 8 illustrates the experimental results of the proposed antenna.

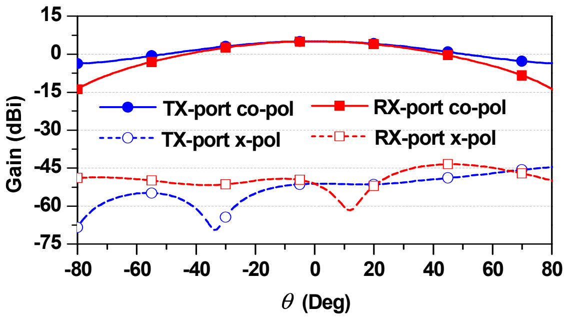

(a)

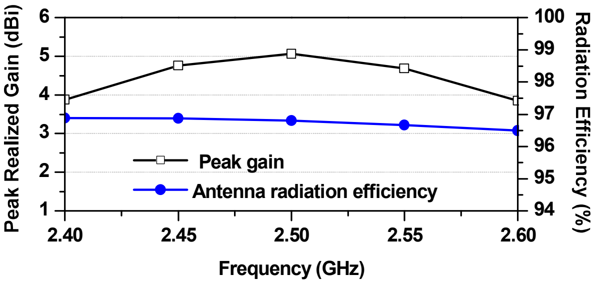

(b)

Fig. 9. Simulated results of a dual-polarized, double differential patch antenna with DGS: (a) co-polarization and cross-polarization E-plane gain patterns for 2.50 GHz and (b) peak realized gain/radiation efficiency.

From measurement, the magnitudes of $|S_{11}|$ and $|S_{22}|$ are determined to be -17.82 dB and -25.77 dB at f_0 = 2.50 GHz, respectively, providing the 10-dB return loss bandwidth of 100 MHz. Similarly, TX-to-RX port isolation is greater than 47 dB for 100 MHz bandwidth.

Fig. 9(a) shows simulated co-polarization and cross-polarization E-plane gain patterns of the proposed antenna. As noted from the figure, the antenna provides better than 5.06 dBi gain and 80° half power beam-width (HPBW) in theta direction of each port. Similarly, the simulated radiation efficiency of the antenna is around 96.5% and 96.8 % at 2.50 GHz for TX- and RX-ports as shown in Fig. 9(b), respectively.

IV. Conclusion

In this paper, microstrip patch antenna with defected ground structure has been demonstrated for in-band full duplex transceiver by deploying two identical branch-line Balun as simple self-interference cancellation circuit. The accurate design equations have been derived to assist in achieving high TX-to-RX port isolation. For experimental demonstration, the antenna has been designed and fabricated at a center frequency of 2.5 GHz. The proposed antenna has achieved higher than 47 dB isolation between TX-to-RX ports with 10 dB return loss of 100 MHz. The easy implementation and good performance indicate that the proposed method can be a good candidate for wideband in-band full duplex systems.

Acknowledgment

This research was supported by the Basic Science Research Program through the National Research Foundation of Korea (NRF) funded by the Ministry of Education, Science and Technology (2016R1D1A1A09918818) and in part by Korean Research Fellowship Program through the National Research Foundation of Korea (NRF) funded by ministry of Science and ICT (2016H1D3A1938065).

References

[1] S. Hong, J. Brand, J. Choi, M. Jain, J. Mehlman, S. Katti, and P. Levis, “Applications of self-interference cancellation in 5G and beyond,” *IEEE Communications Mag*., vol. 52, no. 2, pp. 114-121, Feb. 2014.

[2] M. Mikhael, B. van Liempd, J. Craninckx, R. Guindi, and B. Debaillie, “An in-band full-duplex transceiver prototype with an in-system automated tuning for RF self-interference cancellation,” in *Proc. 1st Int. Conf. 5G Ubiquitous Connectivity*, pp. 110–115, Nov. 2014.

[3] M. Jain, *et al.*, “Practical, real-time, full duplex wireless,” in *Proc. 17th Annu. Int. Conf. Mobile Comput. Netw. (MOBICOM)*, pp. 301–312, 2011.

[4] L. Laughlin, M. A. Beach, K. A. Morris, and J. L. Haine, “Electrical balance duplexing for small form factor realization of in-band full duplex,” *IEEE Communication Mag*., vol. 53, no. 5, pp. 102-110, May 2015.

[5] B. Debaillie, D. Broek, C. Lavin, B. Liempd, E. A. M. Klumperink, C. Palacios, J. Craninkx, B. Nauta, and A. Parssinen, “Analog/RF solutions enabling compact full-duplex radios,” *IEEE Trans. Selected areas in Communication*, vol. 32, no. 9, pp.1662-1673, Sep. 2014.

[6] K. E. Kolodziej, J. G. McMichael, and B. T. Perry, “Multitap RF canceller for in-band full duplex wireless communications,” *IEEE Trans. Wireless Communications*, vol. 15, no. 6, pp. 4321-4333, Jun. 2016.

[7] E. Foroozanfard, O. Franek, A. Tatomirescu, E. Tsakalaki, E. de Carvalho, and G. F. Pedersen, “Full-duplex MIMO system based on antenna cancellation technique,” *IET Electronics Letters*, vol. 50, no. 16, pp. 1116-1117, Jul. 2014.

[8] T. Dinc and H. Krishnaswamy, “A T/R antenna pair with polarization-based reconfigurable wideband self-interference cancellation for simultaneous transmit and receive,” in *Proc. IEEE International Microwave Symposium*, pp. 1-4, 2014.

[9] C. Y. D. Sim, C. C. Chang, and J. S. Row, “Dual-feed dual-polarized patch antenna with low cross polarization and high isolation,” *IEEE Trans. Antennas Propag.*, vol. 57, no. 10, pp. 3405–3409, Oct. 2009.

[10] K. Luo, W.-P. Ding, Y.-J. Hu, and W.-Q. Cao, “Design of dual-feed dual-polarized microstrip antenna with high isolation and low cross polarization,” in *Prog. Electromagn. Research Lett.*, vol. 36, pp. 31–40, Jan. 2013.

[11] H. Nawaz and I. Tekin, “Compact dual-polarized microstrip patch antenna with high interport isolation for 2.5 GHz in-band full-duplex wireless applications,” *IET Microw., Antennas Propag.*, vol. 11, no. 7, pp. 976–981, Jun. 2017.

[12] H. Nawaz and I. Tekin, “Three dual polarized 2.4 GHz microstrip patch antennas for active antenna and in-band full duplex applications,” in *Proc. 16th Medit. Microw. Symp. (MMS)*, Nov. 2016, pp. 1–4.

[13] H. Nawaz, and I. Tekin, “Dual-polarized, differential fed microstrip patch antennas with very high interport isolation for full duplex communication,” *IEEE Trans. Antennas Propagation*, vol. 65, no. 12, pp. 7355-7360, Dec. 2017.

[14] H. Nawaz and I. Tekin, “Double differential fed, dual-polarized patch antenna with 90 dB interport RF isolation for 2.4 GHz in-band full duplex transceiver,” *IEEE Antenna and Wireless Propagation Letters*, vol. 17, no. 2, pp. 287-290, 2018.

[15] P. Kim, G. Chaudhary, and Y. Jeong, “Unequal termination branch-line balun with high-isolation wideband characteristics,” *Microwave Optical Technology Letters*, vol. 58, no. 8, pp. 1175-1178, Aug. 2016.